RSC Advances

PAPER

View Article Online
View Journal | View Issue

Cite this: *RSC Adv.*, 2025, **15**, 44451

Polyurethane coatings reinforced with poly(MMA-*co*-HPMA)@$Mo_2Ti_2AlC_3$ as flexible EMI shielding solutions

Gabriela Toader,†[a] Aurel Diacon,†[a] Martino Aldrigo,[b] Sergiu Iordănescu,[b] Alexandra Mocanu,[bc] Oana Brincoveanu,[b] Cosmin Romanitan,[b] Traian Rotariu,[a] Ovidiu Iorga,[d] Ana-Mihaela Gavrila,[e] Tudor-Viorel Tiganescu*[a] and Edina Rusen*[c]

Lightweight materials, valued for their mechanical strength and efficiency, are widely applied in aerospace, automotive, civil, electronic, and biomedical fields. Recent advances in defense and high-speed communication technologies have intensified interest in their use for electromagnetic interference (EMI) shielding. This study explores the synthesis and characterization of flexible polyurethane (PUR) films embedded with reactive poly(methyl methacrylate-*co*-hydroxypropyl methacrylate)microparticles containing $Mo_2Ti_2AlC_3$ (MXenes). The poly(MMA-*co*-HPMA)@$Mo_2Ti_2AlC_3$ microparticles were prepared *via* suspension polymerization, utilizing the surface hydroxyl functionality to react with isophorone diisocyanate (IPDI) during PUR formation. This ensured uniform dispersion and stable incorporation of MXenes within the matrix. Characterization included FT-IR spectroscopy, SEM, XRD, DMA, mechanical testing, and EMI shielding evaluation. FT-IR confirmed successful copolymerization with complete monomer conversion. SEM revealed the microparticles as a well-dispersed phase within the PUR matrix, while XRD validated the intact MAX phase with minimal delamination. PUR films exhibited high flexibility and tensile resilience, reaching 0.7 MPa at ~85% strain. EMI shielding improved with increasing microparticle concentration, with 2 wt% composites achieving 3 dB attenuation and reflecting 50% more power than lower-loaded samples in the 8.2–12.4 GHz range.

Received 4th August 2025
Accepted 29th September 2025

DOI: 10.1039/d5ra05671c

rsc.li/rsc-advances

1. Introduction

Due to their high strength-to-weight ratio, durability, and efficiency, lightweight materials are used in various domains such as aerospace, automotive, civil engineering, electronics, and biomedical. Among these, special attention is currently given to the development of electromagnetic interference (EMI) shielding due to the various applications in defense and progress of electrocommunication protocols and associated devices. Electronics have been integrated into many aspects of daily life, but they also produce unwanted electromagnetic radiation, or electromagnetic interference (EMI), which can impair the functionality of other electronic devices and their long-term health effects that are still being studied.[1–3]

In the last decade, the development of two-dimensional (2D) atomically thin structures has provided new materials for EMI shielding with performances similar to those of carbon-based nanomaterials, such as MXenes (*e.g.*, metal carbide and nitrides[4]). Consequently, a specific material can be engineered to offer either electromagnetic transparency or EMI shielding properties, depending on the targeted applications.

As a new class of 2D materials, MXenes have received growing attention from the scientific community thanks to their special qualities that warrant their use in a wide range of applications. By selectively etching the aluminum layer, various transition metal-based MXenes that are formed from the pure MAX phase have been studied. Composites based on MXenes materials display good conductivity, high specific surface area, highly active surface sites, and a multilayered structure. These characteristics have made them extremely promising for use in microwave absorption and EMI shielding applications.[5] Furthermore, another appealing aspect of MXenes is their low influence on overall composite weight, leading to their suitability for lightweight materials.

Polyurethanes (PUR) have received increasing attention for composites development due to their versatile properties, such

[a]*Military Technical Academy "Ferdinand I", 39-49 G. Cosbuc Blvd., Bucharest, 050141, Romania. E-mail: viorel.tiganescu@mta.ro*

[b]*National Institute for Research and Development in Microtechnologies—IMT Bucharest, 126A Erou Iancu Nicolae Street, 077190 Bucharest, Romania*

[c]*Faculty of Chemical Engineering and Biotechnologies, National University of Science and Technology Politehnica Bucharest, 1-7 Gh. Polizu Street, Bucharest, 011061, Romania. E-mail: edina.rusen@upb.ro*

[d]*Research and Innovation Center for CBRN Defense and Ecology, 225 Oltenitei, Bucharest, Romania*

[e]*National Institute for Research, Development in Chemistry and Petrochemistry ICECHIM, 202 Spl. Independentei, 060021 Bucharest, Romania*

† Co-first authors, equally contributed to this study.

as high strength and durability, flexibility and elasticity, tailorable morphologies, reactivity, and filler compatibility that can be attained through the control of the polyol and/or diisocyanate component.[6,7] When considering applications connected with the defense sector, the key aspects motivating the use of PUR-based materials are performance, durability, and resilience.[7] PUR materials introduction to the market represented a significant breakthrough, and the class has expanded to include foams (flexible, rigid, fire-resistant), elastomers, binders, coatings, and paints. PUR results from polyaddition reaction involving the polyol and diisocyanate components, including also catalyst species, chain extenders, binders, fillers, *etc.*[6] Through careful selection of polyol and/or isocyanate, drastic changes in the PUR properties can be attained; therefore, the structure-properties correlation between polyol and isocyanate dictates the design of PUR products.[6,7] Depending on the chemical composition of the two components, different morphologies/domains are formed in the resulting PUR. These domains determine properties such as the softness, flexibility, or hardness of the PUR product. As such, PUR-based materials are interesting options for numerous high-performance applications in the defense industry, finding use in body armor, blast mitigation, insulation, sealants, soundproofing, and packaging materials.

Recent advances in dielectric absorber design have emphasized the importance of conduction tailoring (CT) and impedance matching (IM) strategies to attain enhanced electromagnetic wave attenuation. Quan *et al.* demonstrated that thermoplastic elastomer-based films with uniform filler dispersion and chain-bridge effects can significantly improve EM absorption performance.[8] Furthermore, CT was further correlated with the microscopic structure and absorption efficiency.[8] Gradient IM architectures, such as GO/ZIF-67 multilayers, achieved bandwidths up to 13.6 GHz.[9] Dielectric polarization and conduction loss are identified as the primary contributors to the complex permittivity of oxide semiconductors and graphitized carbon, which are crucial in defining their electromagnetic properties.[10] Additionally, solvent evaporation molding with phase change materials has enabled dynamic structural tuning in flexible absorbers, allowing the correlations between EM field polarizations and coherent structures, as well as the determination of rules of the absorption peak generation and frequency shift related to the structural variation.[11]

This study aimed to develop polyurethane (PUR)-based materials with electromagnetic interference (EMI) shielding properties and enhanced mechanical durability, which may serve as specialized coatings. This paper presents a novel approach for developing flexible coatings that provide electromagnetic interference (EMI) shielding. The proposed method involves the use of reactive polymer microparticles, which serve both as reinforcing agents for the PUR matrix and as covering/barrier materials for MXenes. This strategy significantly improves the dispersion of MXenes within the polyurethane matrix. To achieve this, the copolymerization of methyl methacrylate (MMA) and hydroxypropyl methacrylate (HPMA) in suspension in the presence of molybdenum titanium aluminum carbide MAX phase was performed. Thus, using HPMA, the polymer microparticles formed display hydroxyl functional groups, which can react with the diisocyanate component during the synthesis of the polyurethane films. Therefore, the microparticles resulting from the suspension polymerization, which contain the EMI shielding component (MXenes), take part in the PUR synthesis reaction by polyaddition reaction between the polyol and diisocyanate. Another advantage of the selected strategy consists of the encapsulation of MXenes while preserving the MAX phase morphology of the material and its protection from environmental effects.[12] Suspension polymerization proceeds with almost total conversions, using water as the thermal agent that absorbs the reaction heat, and the reaction takes place at the microparticle level. At this stage, there are no phases of separation or precipitation, which makes the reaction compliant with the principles of Green Chemistry.[13] After obtaining the polymeric particles containing the MXenes, they are used as an active reinforcing agent in the PUR synthesis step. Both the synthesis steps for the obtaining of polymer microparticles and their use in polyurethane synthesis as a reinforcing agent are novel approaches for the fabrication of advanced polymer materials.

2. Materials and methods

2.1 Materials

Methyl methacrylate (MMA) (Sigma-Aldrich, Germany) and hydroxypropyl methacrylate (HPMA) (Sigma-Aldrich, Germany) have been purified through vacuum distillation.[14] Azobisisobutyronitrile was purified by recrystallization from methanol, dried under vacuum, and stored in the freezer. Polyvinyl alcohol (PVA) (Sigma-Aldrich, Germany) (M_w = 146 000–186 000 g mol^{-1}, 99+% hydrolyzed), molybdenum titanium aluminum carbide MAX phase $Mo_2Ti_2AlC_3$ (MXenes) (Sigma-Aldrich, Germany) PETOL 56-3 (glycerol–propylene oxide-based polyether polyol triol, M_w = 3000 g mol^{-1}; hydroxyl index 56 mg KOH per g; Chimcomplex S.A, Romania), isophorone diisocyanate (IPDI) (NCO content 37.5%, FairPebTrade SRL, Romania), dibutyl tin laureate (DBTL) (95%, Sigma-Aldrich) were used as received.

2.2 Methods

2.2.1 Suspension polymerization in the presence of $Mo_2Ti_2AlC_3$ MAX phase. In a round-bottom flask, 0.4 g PVA were dissolved in 20 mL of water (solution A). Separately, 0.8 g of $Mo_2Ti_2AlC_3$-MAX phase were dispersed by sonication (10 minutes) in a mixture of 4 g of MMA and 0.4 g of HPMA, followed by the dissolution of 0.05 g AIBN (solution B). Then, solution B was added to solution A, and the reaction mixture was heated at 75 °C under continuous stirring (800 rpm) overnight. Subsequently, the reaction mixture was poured into 600 mL of water, stirred for 1 hour to remove the PVA stabilized, and separated by filtration, followed by several washing cycles with water and finally with methanol. The reaction yield was over 85% (part of the loss was attributed to difficulty recovering smaller particles).

2.2.2 Synthesis of polyurethane (PUR) films containing particles with MXenes resulting from the suspension polymerization. In 8.94 g of PETOL 56-3, different amounts of polymer particles obtained by suspension polymerization (0.052 g (PUR 0.5% MXene), 0.1044 g (PUR 1% MXene), and 0.2088 g (PUR 2% MXene), respectively) were dispersed by sonication (using an Ultrasonic probe Vibracell 250 VCX). Subsequently, 1.5 g of IPDI and 0.06 g DBTL were added to the mixture, followed by stirring for 15 minutes, and pouring into silicon molds. The films were allowed to cure for 72 h at room temperature, followed by curing at 50 °C for 24 h.

Details on characterization methods are included in the SI file.

3. Results and discussions

The first stage of this study consisted in the synthesis of polymer particles containing MXenes ($Mo_2Ti_2AlC_3$) by suspension polymerization. Scheme 1 presents the synthesis steps of the novel materials. There are two major advantages of this approach: (i) utilization of unmodified MAX phase and (ii) the use of HPMA allows access to reactive polymer particles capable of reacting with the diisocyanate component during PUR film fabrication.

Thus, to highlight the suspension copolymerization of MMA and HPMA in the presence of the MXenes component, FT-IR spectroscopy was employed (Fig. 1). Analyzing the results presented in Fig. 1, it can be noticed in the case of polymer particles the presence of the peaks specific for C=O vibration at

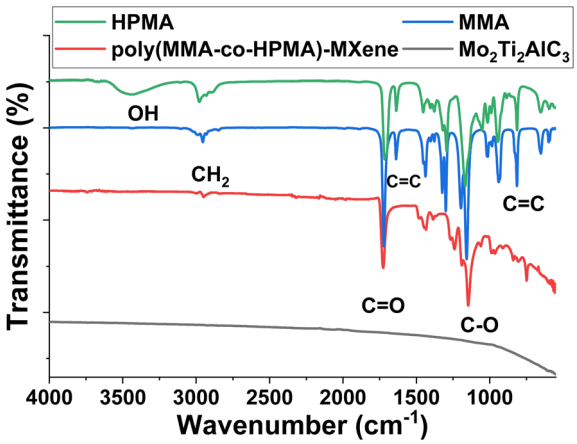

Fig. 1 FT-IR spectra of the MMA (monomer 1), HPMA (monomer 2), poly(MMA-*co*-HPMA)-MXene- polymer particles containing MXenes and of the $Mo_2Ti_2AlC_3$ MAX phase.

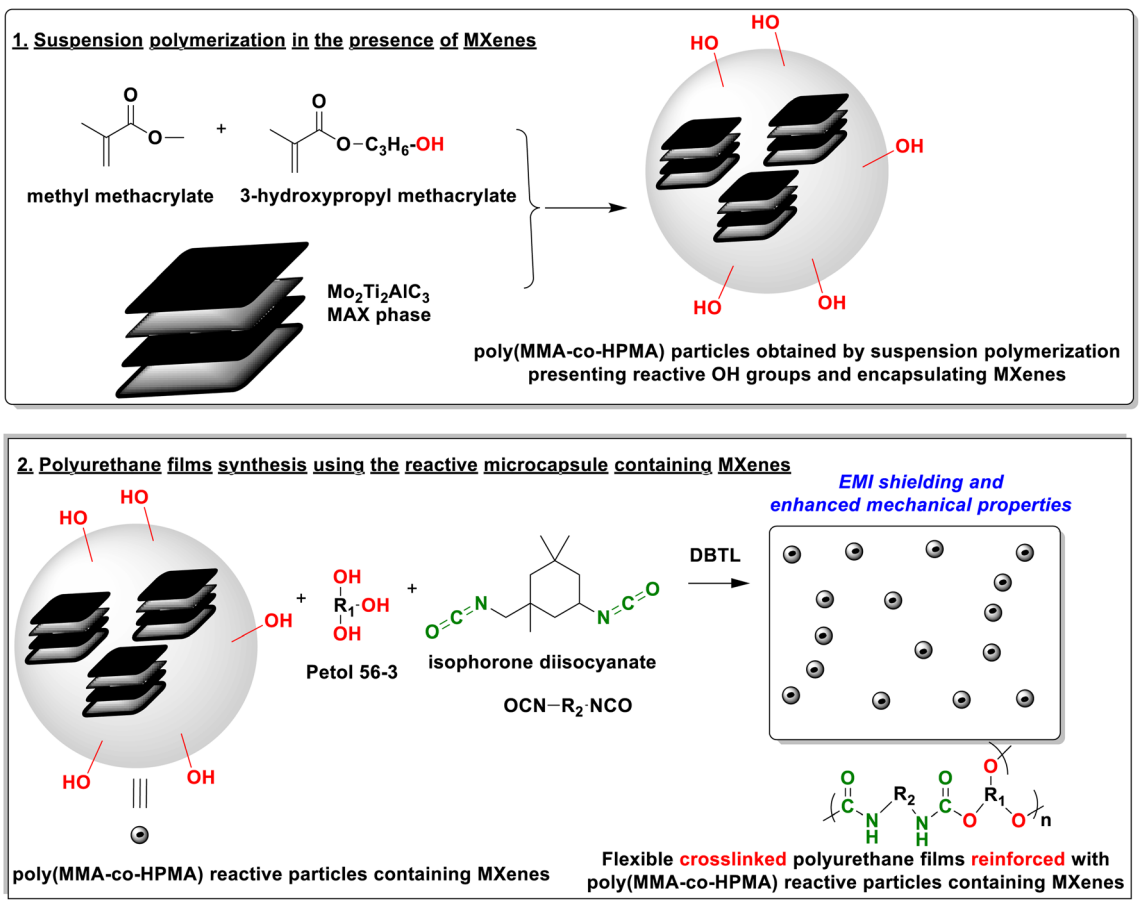

Scheme 1 Concept for using reactive polymer particles containing MXenes as reinforcing agents in polyurethane films and EMI shielding component.

1720 cm^{-1} and C–O–C at 1198 cm^{-1} and 1158 cm^{-1} as well as the signal attributed to the OH vibration at 3500 cm^{-1} specific for HPMA. Furthermore, to confirm the complete conversion, it can be observed that the peaks specific for C=C vibrations at 1638 and 815 cm^{-1} are not present.

To better ascertain the incorporation of the MXenes in the polymer particles, a morphology investigation by optical microscopy and scanning electron microscopy analyses was performed (Fig. 2).

Fig. 2a confirms the presence of MXenes at the interior of the polymer particles, demonstrated by the dark spots in the transparent polymer particles. In Fig. 2b, the harmonica-like structure specific to the unfunctionalized MXenes can be observed, while in Fig. 2c, the MXenes are covered by the polymer within the spherical-shaped polymer particles. RAMAN spectroscopy was employed to assess the structural features of $Mo_2Ti_2AlC_3$ MAX phase and of the copolymer particles resulting from the suspension polymerization. Thus, the spectrum of the pristine MAX phase presents characteristic peaks at 817 cm^{-1} and 992 cm^{-1}, attributed to Mo–C/Ti–C vibrations and Al-layer interactions, respectively.[15] The signals are also present in the case of the polymer particles, confirming the structural integrity of the MAX phase within the polymer matrix. A strong C–H stretching band at 2926 cm^{-1} and a C–H bending vibration at 1444 cm^{-1} are observed, which is consistent with the presence of the copolymer.[16] It must be noted that the absence of *D* (~1350 cm^{-1}) or *G* (~1580 cm^{-1}) bands indicates the absence of exfoliated carbonaceous species and suggests that the MAX phase remains in its 3D arrangement[17] (Fig. 3).

The RAMAN results imply that the suspension polymerization led to a minimal disruption of the MAX phase and to further sustain this aspect XRD analysis was performed to evaluate the exfoliation process (Fig. 4).

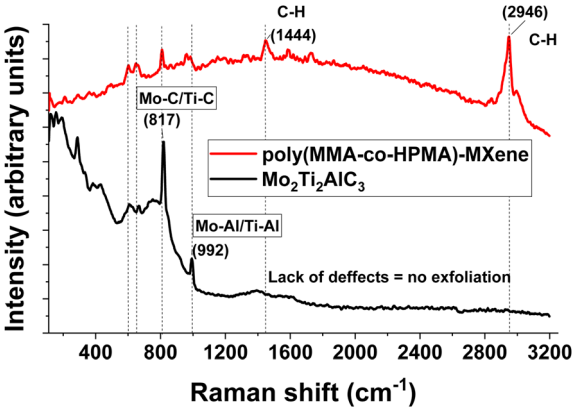

Fig. 3 RAMAN spectra for $Mo_2Ti_2AlC_3$-MAX phase (commercial) and for the poly(MMA-*co*-HPMA) microparticles obtained in suspension in the presence of MAX phase.

From the analysis of Fig. 4 it can be determined the MXenes diffraction pattern remains unchanged from the initial commercial MAX phase to the polymer particles with MXenes. Thus, it can be deducted that the MXenes remain compact with limited delamination and/or exfoliation.[18,19] For the polymer particles sample the additional signals at 15° and 30° are specific for the PMMA-based polymer matrix.[20,21]

The next step of this study consisted in the synthesis of PUR films through the polyaddition reaction between a diisocyanate and a polyol, respectively the polymer particles presenting reactive hydroxyl groups on their surface. Thus, the polymer

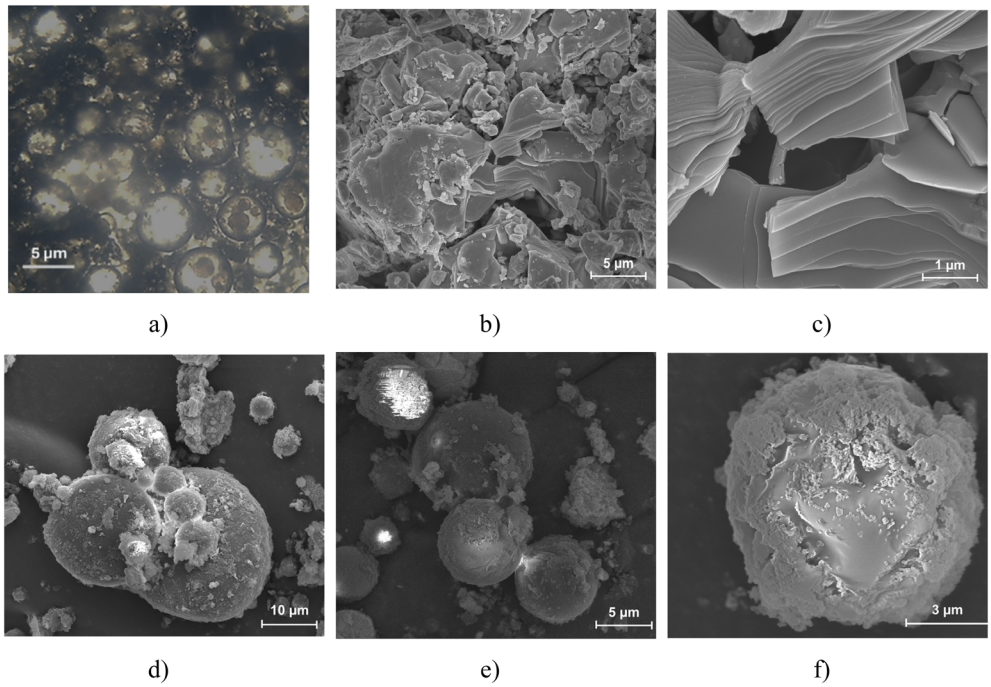

Fig. 2 Morphology characterization of the samples: (a) optical microscopy of the polymer particles; (b) and (c) SEM images of the $Mo_2Ti_2AlC_3$ MAX phase; (d–f) SEM analysis of the poly(MMA-*co*-HPMA)-MXene polymer microparticles containing MXenes.

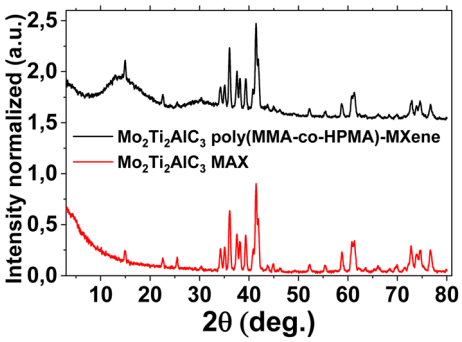

Fig. 4 XRD diffraction pattern for $Mo_2Ti_2AlC_3$-MAX phase (commercial) and for the polymer microparticles obtained in suspension in the presence of MXenes.

particles can act as a reinforcing agent taking part in the polymerization reaction. To highlight the successful polyaddition polymerization reaction FT-IR analysis was performed (Fig. 5). The data presented in Fig. 5 confirms the complete reaction of NCO groups with no residual signal being registered[22] at 2245 cm^{-1}, while for the hydroxyl group from the polyol PETOL 56-3, no residual signal is present confirming the complete consumption.

To highlight the polymer particles containing MXenes in the PUR matrix, the morphology of the films was investigated by SEM (Fig. S1).

Based on the SEM images presented in Fig. S1, it can be confirmed that the polymer particles are well distributed in the PUR matrix, leading to the formation of two different phases, PUR matrix as the continuous phase, while the suspension particles form the dispersed phase. Thus, the synthesis stage successfully demonstrated a straightforward and efficient method for fabricating polyurethane films, in which PUR serves as the continuous phase and the polymer particles act as the dispersed reactive phase facile. The main drawback remains however the price of MXenes, but overall, the fabrication strategy/method is relatively economical offering the possibility for longer lifetime/service for the MXenes component due to the encapsulation in poly(MMA-*co*-HPMA) polymer particles. The obtained polyurethane coatings could also allow the possibility for encapsulated MXenes recovery and reutilization.

The next step in the material characterization involved the use of dynamic mechanical analysis (Fig. 6) to ascertain the influence of the filler (polymer particles encapsulating MXenes obtained by suspension polymerization) on the glass transition temperature and the mechanical characteristics of the PUR films.

Dynamic mechanical analysis revealed a single dominant α-transition associated with the soft-segment glass transition, with tan δ peaks (T_g values) shifting from −44 °C (PUR) to −45 °C (PUR + 1% MXene) and −38 °C (PUR + 2% MXene). The slight downward shift at 1% suggests minor plasticization, whereas the upward shift at 2% indicates increased chain restriction due to strong polyurethane-poly(MMA-*co*-HPMA)@$Mo_2Ti_2AlC_3$ particles interactions.[23,24] Both composites exhibited reduced tan δ_{max} compared to neat PUR, reflecting lower viscous losses at the peak, with the 1% sample showing the highest suppression.[25] Nevertheless, the PUR + 2% MXene displayed a broader tan δ peak which implies a wider relaxation time distribution and enhanced damping over a broader temperature range.[23,25] These trends indicate that the energy dissipation arises mainly from segmental α-relaxation, interfacial friction, and reversible

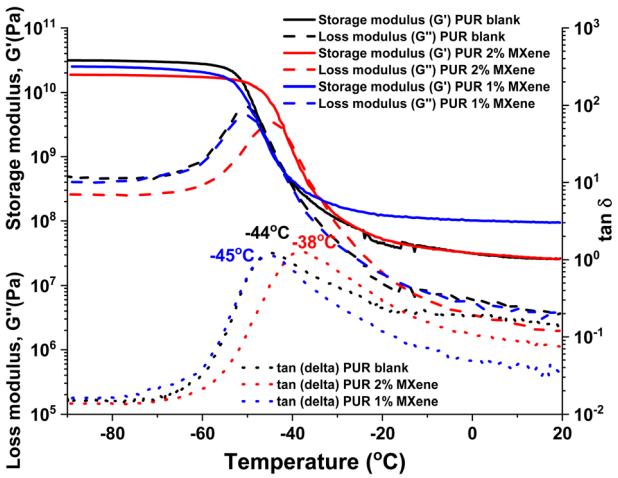

Fig. 6 DMA analysis results for the blank and modified PUR with MXenes.

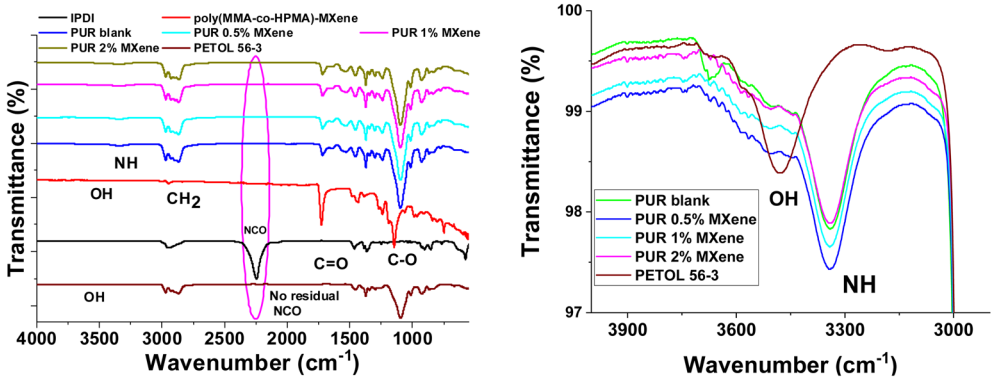

Fig. 5 FT-IR analysis of the PUR films containing different concentrations of polymer particles (poly(MMA-*co*-HPMA)-MXene), isophorone diisocyanate (IPDI) and polyol PETOL 56-3.

hydrogen bonding with higher poly(MMA-*co*-HPMA)@$Mo_2Ti_2AlC_3$ particles loading promoting interfacial energy dissipation while simultaneously constraining polymer mobility.[23,24]

All composite polyurethane (PUR) films, despite variations in their composition, demonstrate remarkable flexibility even at low temperatures. This quality is particularly beneficial for applications requiring electromagnetic interference (EMI) shielding, where maintaining pliability is essential for effective performance across various environmental conditions. The capacity of these films to preserve their elastic properties enhances their functionality in protective applications, ensuring they adapt well to surfaces while delivering reliable shielding performance.

In light of the potential applications of polyurethane (PUR) reinforced with poly(MMA-*co*-HPMA)@$Mo_2Ti_2AlC_3$ reactive particles, it was essential to conduct further mechanical testing to ascertain their performance and reliability.

The tensile tests were conducted on the blank PUR films and the samples reinforced with poly(MMA-*co*-HPMA)@$Mo_2Ti_2AlC_3$ reactive particles. Fig. 7 shows that for a similar ultimate stress value (~0.7 MPa), the maximum strain values decreased as the MXenes content increased. The reduction in strain values suggests an increase in stiffness and structural integrity of the composite films. This enhancement is advantageous for EMI shielding applications, as a slightly stiffer material can better maintain its shape and functionality under mechanical stress for longer, ensuring consistent electromagnetic wave attenuation in various operating conditions.

In an oscillatory test, the time-dependent behavior of a sample can be assessed by varying the frequency of the applied stress or strain within the non-destructive deformation range. An appropriate mechanical model for characterizing gel-like behavior is a spring in parallel with a Maxwell element.[26,27] Viscoelastic solids and gel-like systems both show yield stress behavior. This means that they need to break their internal structure before they can flow freely. Fig. S2 illustrates the dependence of log G', G'' on the log ω for PUR.

In the linear viscoelastic region (LVER), the applied stresses are insufficient to induce structural breakdown (yielding), allowing for the measurement of microstructural properties. When the applied stress surpasses the yield stress, non-linear behaviors emerge, making it challenging to correlate measurements with microstructural characteristics. The linear viscoelastic region can be identified through an experiment by conducting a stress or strain sweep test and observing the point at which the structure begins to yield (Fig. 8a). This marks the point where G' becomes dependent on stress or strain. The storage modulus (G') exceeds the loss modulus (G''), indicating the crosslinked nature of the PUR films.[28] The increase of G' can likely be attributed to enhanced molecular aggregation that resulted in a more rigid structure.[29,30]

To demonstrate a viable utilization direction for the obtained coatings the next characterization steps involved the evaluation of EMI shielding characteristics which represent an appealing valorization route for s based composites.[4,5,18,19,33–36] The results obtained for EMI shielding experiments are presented in Fig. 9.

To assess the EMI shielding properties of the MUTs ("Reference-PUR Blank", "0.5%", "1%", and "2%") we used a calibrated VNA (Vector Network Analyzer) connected to two X-band waveguide transitions, and in between the latter we inserted the various MUTs to register the S parameters at the two ports of the VNA. Using the measured S parameters (Fig. 9a), we can extract all the quantities of eqn (1)–(4) from SI file.

Fig. 9b–d show that reference (PUR blank) (solid black line) and sample 1% (solid blue line) exhibit very similar values for SE_A, SE_R, and SE, respectively; this means that the addition of suspension particles containing MXenes does not entail a monotonic change of sample's performance in terms of EMI shielding. This could be ascribed in principle to a disordered dispersion of suspension particles containing MXenes in the polymeric matrix. The sample 0.5% is even better than the Reference (PUR blank) and sample 1%, for both transmission and reflection, *i.e.*, sample 0.5% is the most EM transparent material. Even if all the characterized samples exhibit good transmission and reflection properties ($|S_{21}|$ is always between −1 and −2 dB, whereas $|S_{11}|$ is always between −6 and −13 dB), an evident attenuation can be observed in $|S_{11}|$ around 10 GHz when considering sample 0.5% and sample 2%. The sample with 2% content of suspension particles containing MXenes is the one that reflects the most EM radiation passing through the waveguides, with an attenuation of almost 3 dB with respect to sample 0.5%, meaning that sample 2% reflects almost 50% more power compared to sample 0.5%. These outcomes are consistent with Fig. 9b–d, which demonstrate that sample 2% offers the best EMI shielding performance, with SE attaining values always between 1 and 1.5 dB over the whole X band. It is interesting to observe the results for the conductivity (Fig. 9e): sample 2% is the most conductive one, with σ reaching more than 13 S m^{-1} at 12 GHz and being always greater than 9 S m^{-1}. This value is almost 3× greater than the conductivity of sea water, which is about 5 S m^{-1}. A simple explanation for these results is that the absorption of the incident EM waves could be related to the moisture content of the MUTs, but the enhancement of the conductivity comes from the concentration of

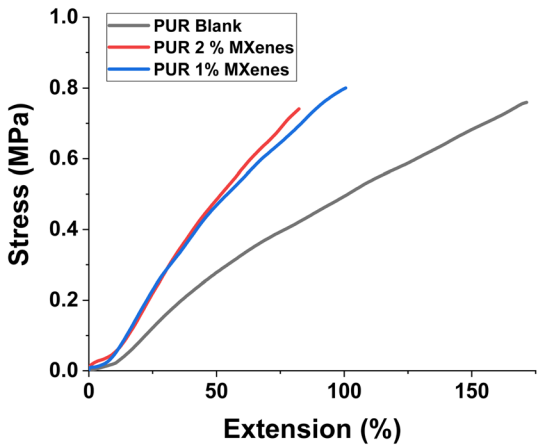

Fig. 7 Stress–strain dependence for PUR and PUR reinforced with poly(MMA-*co*-HPMA)@$Mo_2Ti_2AlC_3$ reactive particles.

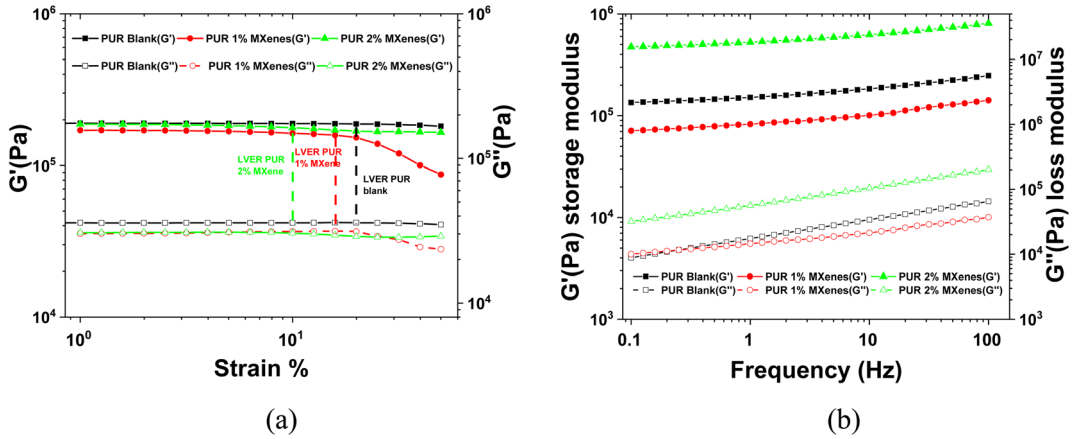

Fig. 8 Shear tests for PUR and PUR with MXenes: (a) the dependence of G', G'' to the strain; (b) the dependence of G', G'' to the frequency; (b) displays the dependence of G', G'' to the frequency. In the applied frequency range (0.1–100 Hz), the G' and G'' moduli increased slowly with increasing frequency. This illustrates that all the samples could maintain a weak gel-like behavior. In weak gel, $G' > G''$ in all frequencies, and the two curves move parallel to each other and are dependent on frequency. In strong or real gel, also $G' > G''$, but the slope of the curves of G' and G'' moduli are zero, and the moduli are not dependent on frequency.[31,32]

suspension particles containing MXenes. Finally, the values of the skin depth (Fig. 9f) are strictly related to those of the conductivity, for the following reason: from eqn (4), an increase of σ entails a decrease of δ and, most of all, a general rule of thumb for any conductive material is to have a thickness which is at least double with respect to its skin depth, to prevent the penetration of the high-frequency EM field inside the materials itself and, hence, additional losses. Since the thickness of all MUTs spans between 1.64 and 2.27 mm, it is evident that the skin depth has an abrupt decrease for increasing frequencies

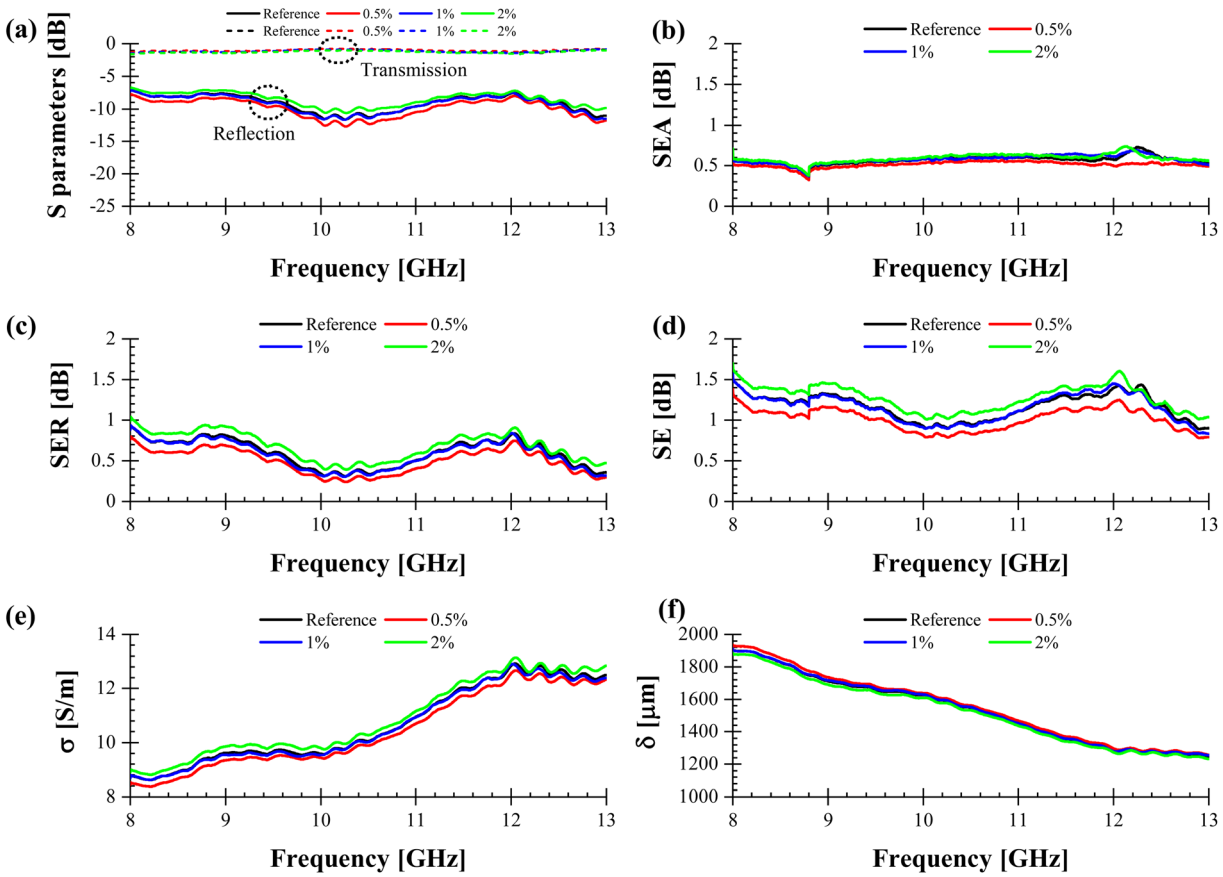

Fig. 9 (a) Measured S parameters. Extracted (b) SE_A, (c) SE_R, (d) SE, (e) conductivity, and (f) skin depth for all the MUTs in the X band.

since the thickness of each sample becomes much greater than the corresponding skin depth.

As a whole, sample 2% has the potential to be a good EMI shielding material and we expect that a further increase of the suspension particles containing MXenes content will enhance the shielding properties, by keeping at the same time an acceptable degree of flexibility. The latter characteristic is an added value since it can follow the shape of the object to shield it from EMI. We stress here that for all the MUTs described in this work, the results are consistent and reproducible after systematic measurements.

The increase in shielding capacity with a higher concentration of MXenes in the polymer capsule can be explained by phase segregation. This phase segregation enhances multiple reflection stages within the absorbed frequency domain, as illustrated in Fig. S3.

The observed performance trends can be directly correlated with the composition and structural characteristics of the PUR composites. As the content of polymer particles containing $Mo_2Ti_2AlC_3$ increases, the dispersion within the PUR matrix becomes more heterogeneous, as seen in SEM images (Fig. S1), leading to phase segregation that enhances multiple internal reflections (Fig. S3). This structural evolution contributes to improved EMI shielding performance (Fig. 9d), with the 2 wt% sample showing the highest conductivity and lowest skin depth (Fig. 9e and f). Simultaneously, mechanical tests (Fig. 7) reveal increased stiffness and reduced strain, indicating stronger interfacial interactions between the matrix and the encapsulated $Mo_2Ti_2AlC_3$. These findings confirm that the composition directly influences the microstructure, which in turn governs the mechanical and electromagnetic properties of the films.

4. Conclusions

This study presented the synthesis and characterization of flexible polyurethane films incorporating poly(methyl methacrylate-*co*-hydroxypropyl methacrylate) reactive particles containing $Mo_2Ti_2AlC_3$ MAX phase. The particles obtained have hydroxyl functional groups capable of reacting with the diisocyanate during the formation of polyurethane films. Thus, the straightforward synthetic approach allows encapsulation of MXenes without disrupting the MAX phase, as confirmed by XRD analysis, and facilitates efficient dispersion and integration of the poly(MMA-*co*-HPMA) microcapsules in polyurethane films. The mechanical properties of the PUR films were assessed by DMA analysis, shear, and tensile tests. The main advantages of the obtained materials are their flexibility and strain resistance. The EMI shielding characteristics measurements revealed that the performance of the samples improved with the increase in polymer capsule content. This can be attributed to an efficient phase distribution of the MXenes contained in the polymer particles, which enhances a multiple-stage reflection process of the microwaves inside the PUR films. Thus, the results obtained in this study establish an experimental foundation for the development of lightweight multifunctional PUR films, which already exhibit favorable preliminary characteristics for electromagnetic interference (EMI) shielding and show promising mechanical resilience for potential shock mitigation applications. Additionally, the effective encapsulation of the MXenes MAX phase within polymer-based particles contributes to its structural integrity and long-term stability. These findings highlight the relevance and applicability of the current material design, while further optimization in future studies is expected to refine and enhance their performance, unlocking broader functionalities for advanced protective technologies.

Conflicts of interest

There are no conflicts to declare.

Data availability

All data supporting the findings of this study are available within the article and its supplementary information (SI) files. Supplementary information: description of characterization methods, Fig. S1 – SEM images for the polyurethane coatings containing different concentrations (wt%) of polymer particles containing MXenes; Fig. S2 – The dependence of $\log G'$, G'' on the $\log w$ for PUR and Fig. S3 – The mechanism of EMI shielding. See DOI: **https://doi.org/10.1039/d5ra05671c**.

Acknowledgements

This work was supported by grants of the Ministry of Research, Innovation and Digitization, CNCS UEFISCDI, project number PN-IV-P2-2.1-TE-2023-0806 ctr. 55 TE/2025 and project number PN-IV-P7-7.1-PTE-2024-0486 ctr. no. 1PTE/2025, within PNCDI IV. IMT team would like to thank for financial support in part by the Romanian Ministry of Research, Innovation, and Digitization through the Core Program within the National Research, Development and Innovation Plan 2022–2027, under Project 2307 – μNanoEl, contract number 8N/03.01.2023, and partial financial support through the project "National Platform for Semiconductor Technologies", contract no. G 2024-85828/390008/27.11.2024, SMIS code 304244, co-funded by the European Regional Development Fund under the Program for Intelligent Growth, Digitization, and Financial Instruments. ICECHIM acknowledges a grant of the Ministry of Research, Innovation and Digitalization, CNCS—UEFISCDI, project number PN-IV-P2-2.1-TE-2023-1293, 40 TE/2025 (Drug-Scan), within PNCDI IV.

References

1 X.-Y. Wang, S.-Y. Liao, Y.-J. Wan, P.-L. Zhu, Y.-G. Hu, T. Zhao, R. Sun and C.-P. Wong, *J. Mater. Chem. C*, 2022, **10**, 44–72.
2 L. Hardell and C. Sage, *Biomed. Pharmacother.*, 2008, **62**, 104–109.
3 W. R. Adey, *J. Cell. Biochem.*, 1993, **51**, 410–416.
4 F. Shahzad, M. Alhabeb, C. B. Hatter, B. Anasori, S. Man Hong, C. M. Koo and Y. Gogotsi, *Science*, 2016, **353**, 1137–1140.

5 R. Kumar, S. Sahoo, E. Joanni and J.-J. Shim, *Compos. B Eng.*, 2023, **264**, 110874.
6 J. O. Akindoyo, M. D. H. Beg, S. Ghazali, M. R. Islam, N. Jeyaratnam and A. R. Yuvaraj, *RSC Adv.*, 2016, **6**, 114453–114482.
7 A. Das and P. Mahanwar, *Adv. Ind. Eng. Polym. Res.*, 2020, **3**, 93–101.
8 B. Quan, Y. Chen, Y. Wang, X. Lu, T. Guo, M. Zhang and X. Huang, *Carbon*, 2023, **206**, 392–401.
9 B. Quan, Y. Wang, Y. Chen, M. Zhang, J. Liu, Q. Jia, X. Lu, J. Chen and X. Huang, *J. Mater. Chem. A*, 2023, **11**, 3625–3631.
10 B. Quan, W. Shi, S. J. H. Ong, X. Lu, P. L. Wang, G. Ji, Y. Guo, L. Zheng and Z. J. Xu, *Adv. Funct. Mater.*, 2019, **29**, 1901236.
11 Y. Chen, B. Quan, J. Liu, X. Lu, L. Lin, G. Shao, Y. Wen, R. Jin, X. Shen and X. Huang, *ACS Appl. Mater. Interfaces*, 2025, **17**, 9748–9759.
12 R. A. Soomro, P. Zhang, B. Fan, Y. Wei and B. Xu, *Nano-Micro Lett.*, 2023, **15**, 108.
13 P. T. Anastas and J. C. Warner, *Green Chemistry: Theory and Practice*, Oxford University Press, 2000.
14 W. T. K. Stevenson, R. A. Evangelista, R. L. Broughton and M. V. Sefton, *J. Appl. Polym. Sci.*, 1987, **34**, 65–83.
15 B. Anasori, M. Dahlqvist, J. Halim, E. J. Moon, J. Lu, B. C. Hosler, E. a. N. Caspi, S. J. May, L. Hultman, P. Eklund, J. Rosén and M. W. Barsoum, *J. Appl. Phys.*, 2015, **118**, 094304.
16 D. Bertoldo Menezes, A. Reyer, A. Benisek, E. Dachs, C. Pruner and M. Musso, *Phys. Chem. Chem. Phys.*, 2021, **23**, 1649–1665.
17 M. Khazaei, A. Ranjbar, K. Esfarjani, D. Bogdanovski, R. Dronskowski and S. Yunoki, *Phys. Chem. Chem. Phys.*, 2018, **20**, 8579–8592.
18 E. Rusen, A. Mocanu, O. Brincoveanu, A. Boldeiu, C. Romanitan, M. Aldrigo, S. Iordănescu, A. Diacon, G. Toader and R. Gavrila, *J. Mater. Chem. C*, 2024, **12**, 11586–11593.
19 E. Rusen, A. Mocanu, G. Toader, A. Diacon, C. Romanitan, O. Iorga, M. Aldrigo, C. Parvulescu, R. Mitran and O. Brincoveanu, *RSC Adv.*, 2024, **14**, 37202–37215.
20 Y. Ul Haq, I. Murtaza, S. Mazhar, N. Ahmad, A. A. Qarni, Z. Ul Haq, S. A. Khan and M. Iqbal, *J. Appl. Polym. Sci.*, 2020, **137**, 49197.
21 A. Diacon, E. Rusen, F. Rizea, A. Ghebaur, D. Berger, R. Somoghi, A. Matei, P. Palade and O. Tutunaru, *Eur. Polym. J.*, 2021, **152**, 11.
22 H. Gong, X. Guo, D. Cao, P. Gao, D. Feng, X. Zhang, Z. Shi, Y. Zhang, S. Zhu and Z. Cui, *J. Mater. Chem. B*, 2019, **7**, 744–754.
23 H. L. Ornaghi, L. K. Lazzari, E. F. Kerche and R. M. Neves, in *Mechanics of Nanomaterials and Polymer Nanocomposites*, ed. H. Abdellaoui, S. M. R. and S. Siengchin, Springer Nature Singapore, Singapore, 2023, pp. 147–161, DOI: **10.1007/978-981-99-2352-6_8**.
24 R. Sanaka, S. K. Sahu, P. S. R. Sreekanth, J. Giri, F. Mohammad, H. A. Al-Lohedan, M. S. Saharudin and Q. Ma, *Polymers*, 2025, **17**, 338.
25 N. Warasitthinon and C. G. Robertson, *Rubber Chem. Technol.*, 2018, **91**, 577–594.
26 B. Kılıçarslan, I. Bozyel, D. Gökcen and C. Bayram, *Macromol. Mater. Eng.*, 2022, **307**, 2100978.
27 K. S. Fancey, *J. Mater. Sci.*, 2005, **40**, 4827–4831.
28 A. H. Williams, S. Roh, A. R. Jacob, S. D. Stoyanov, L. Hsiao and O. D. Velev, *Nat. Commun.*, 2021, **12**, 2834.
29 J. Somberg, G. Gonçalves, M. S. Sánchez and N. Emami, *Mater. Des.*, 2022, **224**, 111304.
30 M. Gao, W. Wang, J. Hou and L. Ye, *Aggregate*, 2021, **2**, e46.
31 Y. Ren, L. Jiang, W. Wang, Y. Xiao, S. Liu, Y. Luo, M. Shen and J. Xie, *Food Hydrocolloids*, 2020, **99**, 105371.
32 L. Wang, H.-M. Liu, C.-Y. Zhu, A.-J. Xie, B.-J. Ma and P.-Z. Zhang, *Carbohydr. Polym.*, 2019, **209**, 230–238.
33 S. Soman, S. Kulkarni, A. Pandey, N. Dhas, K. S. Shirur, R. S. Gude, S. M. Vidya, S. Nayak, S. D. George and S. Mutalik, *Mater. Today Commun.*, 2024, **38**, 107711.
34 B. Anasori, Y. Xie, M. Beidaghi, J. Lu, B. C. Hosler, L. Hultman, P. R. C. Kent, Y. Gogotsi and M. W. Barsoum, *ACS Nano*, 2015, **9**, 9507–9516.
35 R. Akhter and S. S. Maktedar, *J. Materiomics*, 2023, **9**, 1196–1241.
36 S. Das, S. Sharma, T. Yokozeki and S. Dhakate, *Compos. Struct.*, 2021, **261**, 113293.